Geotectonics, Vol. 39, No. 2, 2005, pp. 143–155. Translated from Geotektonika, No. 2, 2005, pp. 52–65.

Fault Systems and Stress Fields in the Southern Dead Sea Rift

O. V. Lunina
Institute of the Earth's Crust, Siberian Division, Russian Academy of Sciences, ul. Lermontova 128, Irkutsk, 664033 Russia
e-mail: lounina@crust.irk.ru
Received January 12, 2004

Abstract—Fractures and fault zones are studied in the Dead Sea Rift with geological and structural methods. As is established from the statistical processing of the data, the N–S- and NW-trending faults control the structure in the southern portion of this rift. They are the longest and accompanied by the thickest crush zones and the most developed fracture systems in comparison with faults oriented in other directions. The roughly meridional trend of fracture systems is vividly expressed within basins and often shaded by other fracture systems in the interbasin links. Mesostructural marks indicate the normal faulting along master faults within local basins, while between them, in uplifted offsets, the displacements may change from normal to strike-slip within the same fault zone. The NW-trending faults are characterized by normal and combined normal and strike-slip displacements; the E–W faults reveal lateral displacement, and the NE-trending faults exhibit strike-slip and normal displacements. Two local stress fields equal in implications for the tectonic evolution of the Dead Sea Rift have been reconstructed from the fracture patterns: (1) E–W (predominant) and ENE extension and (2) shear accompanied by the NE or less developed E–W extension and the NW or less developed N–S compression. Comparison of the results obtained with analog models of structural systems formed under various loading conditions shows that the specific features of faulting and stress fields in the Dead Sea Rift resulted from oblique extension.

INTRODUCTION

The Dead Sea Rift[1] extends for 1000 km from the Red Sea in the south to the East Anatolian Fault in the north (Fig. 1). It consists of a series of basins with uplifted margins bounded by steeply dipping faults. The major basins in the southern portion of the rift include the Gulf of Elat (Aqaba), the Arava Valley, Lake Kinneret, and the Hula Basin (Fig. 2). In the north, they extend as the Lebanese Fault System, and the El Ghab and Karasu basins. The local basins are separated by links, where the fault-pattern is expressed in topography less explicitly.

This region is the object of numerous structural, geological, and geophysical studies. Some of these were focused on stress fields. Nevertheless, the origin and geodynamics of the Dead Sea Rift remain a hotly debated subject, and its propagation in the meridional direction is ascribed to several possible mechanisms: (1) E–W extension [18, 28], (2) NE extension [19], (3) meridional compression [23], and (4) NNW compression combined with ENE extension [17]. Like other fault systems characterized by transtensional tectonics, this structure reveals a variety of local stress fields, which have lead researchers to different interpretations. In particular, some of them regard the Dead Sea Rift as a transform fault [18, 19] while others consider the same structure to be a pure rift [21]. From the third viewpoint, the effects of normal and strike-slip faulting are assumed and it is supposed that the Dead Sea Rift is a result of oblique extension [25, 28]. Dozens of controversial facts were pointed out in numerous works as evidence for one model or another of the Dead Sea Rift's evolution. In particular, mechanisms of local basin formation were discussed and amplitudes of strike-slip displacements along different rift segments were estimated [3, 4, 20]; however, little attention was paid to fault patterns. At the same time, it is known that any fault system of certain origin is characterized by an intrinsic structure that reflects its formation conditions [8]. Some historical information on the faults of this territory is briefly given hereafter.

The fault pattern of the Dead Sea Rift and its adjacent territory is controlled by faults of several directions that have variable ages and different present-day activities. The N–S- and NNW-trending normal faults and nearly latitudinal strike-slip faults were formed in the late Miocene and Pliocene during the Eritrean Stage [21]. It is commonly suggested that this phase was characterized by minimal uplift of walls and widespread volcanic activity. However, some authors pointed out that the W–E dextral strike-slip faults and auxiliary NW- and NE-oriented faults were largely formed during exactly the Eritrean Stage [27]. The Levantine Stage, active from the late Pliocene and Pleistocene, formed the Dead Sea Rift and its uplifted shoulders. The nearly latitudinal strike-slip faults might have compensated for extension of the rift during this period [21]. The NW- and NE-trending faults that locally offset from the Dead Sea, Lake Kinneret, and Hula basins, having a crescent shape in plan,

[1] The traditional name of this rift system adopted in the majority of publications is used in this article. The Dead Sea Rift is also called the Levant Rift or Levant Fault Zone, the Levant Rift System, and transform fault of the Dead Sea.

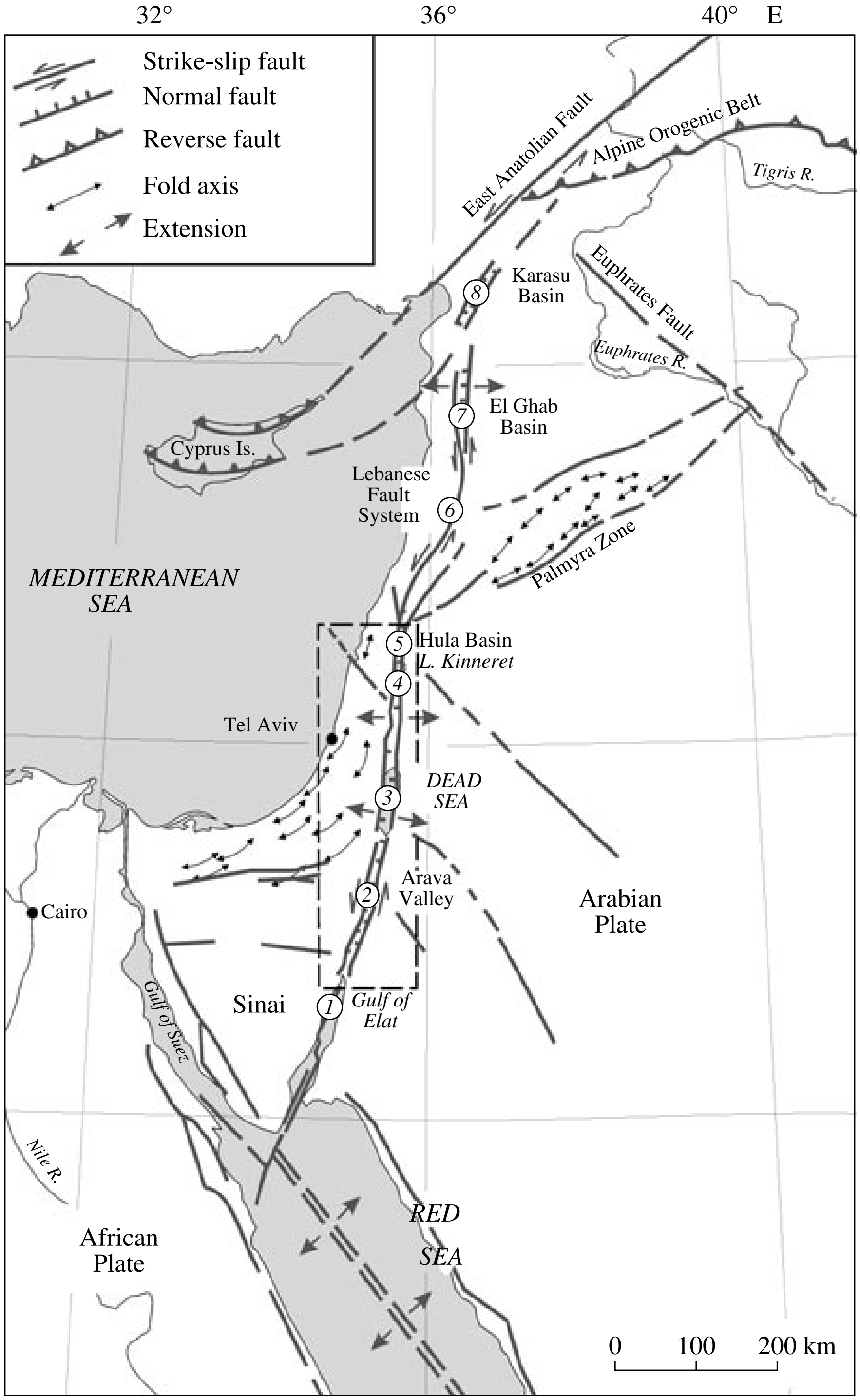

Fig. 1. Tectonic setting of the Dead Sea Rift, modified after [14]. Box is the study area. Numerals in circles designate locations of local basins and fault systems in the Dead Sea Rift; their names are inscribed in the map.

are also related to the rift stage [21, 22]. It should be noted that the fault patterns shown in different maps [29, 35, etc.] are markedly distinct. One of these recently published structural schemes is reproduced in Fig. 3; however, it also does not cover the entire rift zone.

Thus, the implication of particular faults in the structure of the Dead Sea Rift remains uncertain and thus serves as one of the causes of ambiguity in recognition of its tectonic origin. Therefore, this study is focused on the fault systems, the most typical stress fields within the rift, and the prevalent orientation of their principal axes. The importance of such work is evident, because features of the last and current stages in the tectonic history of any region leave their imprints

Fig. 2. General view of major basins in the southern Dead Sea Rift: (A) eastern wall of the Arava Valley, (B) western wall of the Dead Sea Basin, and (C) view of the eastern wall of the Hula Basin in northern Israel.

on fault patterns and topography. In turn, the state of stress is one of the main factors that determines the geodynamic regime and further evolution of a territory.

RESULTS OF STRUCTURAL INVESTIGATIONS AND STATISTICAL PROCESSING OF DATA

The structure has been studied within the Dead Sea Rift from the Gulf of Elat to the Hula Basin. At each of 20 stations (Fig. 4), the fracture patterns and fault zones were subjected to detailed study, relationships between fracture systems were characterized, and displacements of markers and slickensides were measured. The results of fracture orientation measurements at 16 stations were plotted on diagrams. In total, including the data on striation and marker displacements, more than 1600 measurements have been made. Only those fractures whose tectonic origin did not cast any doubt were used in field observations. These fractures reveal systematic distribution, are straight-line, and are regularly arranged in space relative to one another [6]. The exact timing of fractures is most problematic. Nevertheless, experience in the study of tectonic fractures in various stratigraphic complexes of seismically active regions and their reliable correlation enable recognition of superimposed deformations and relatively young fractures that were formed or reactivated by movements along active faults [2, 7, 27]. The results presented in this article pertain to the fractures and fault zones traceable in crystalline and sedimentary rocks varying in age from Precambrian to Pleistocene.

Orientation and Significance of Fault Systems

The maximums in the diagrams of fracture density (Fig. 4) indicate that the nearly meridional rift direction of faults either is the main direction or is at least equal to the others at nine stations (0101, 0302, 0401, 0402, 0501, 0602, 0604, 0702, and 0703) and generally prevails over other systems in the southern Dead Sea Rift (Fig. 5A, see rose diagram). The submeridional fractures are often steeply dipping (70–80°) and bear indications of nearly vertical displacements as follows from downfaulting of markers (Fig. 6A) and striations oriented downdip the fracture plane (Fig. 6B). In only one place (Station 0702) was there noted a displacement in the walls of the old Templar Castle of Vadum Iacob, which is situated a little to the south of the Hula Basin (Fig. 7A); this displacement was 0.5 m in the horizontal direction (measured at one point). The previously mentioned left-lateral separation of 2.1 m [40] is probably a cumulative value comprising measurements of several fault segments. At the same time, the most deformed wall bears signs of oblique displacement (Fig. 7B). The maximum gap here is 0.28 m, the left-lateral separation is 0.23 m, and the normal separation is 0.07 m. Down the slope of the fortress walls, at the foot of one step of

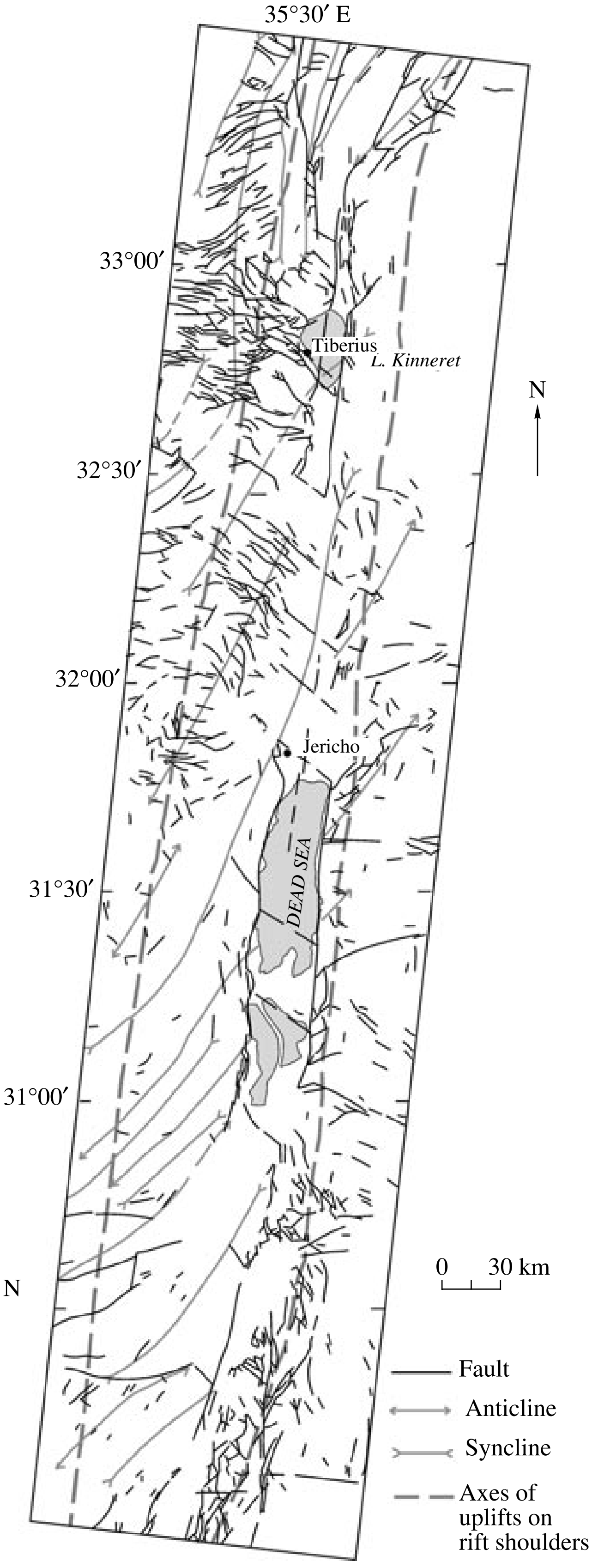

Fig. 3. Structural scheme of the Dead Sea Rift, after [18].

the fault escarpment (Fig. 7C), a normal fault zone 1.0–1.5 m in apparent thickness (dip azimuth 90° ∠60°) was traced in the Pleistocene sandstone containing gravel. Approximately 15 km northeast of the Templar Castle of Vadum Iacob, a separation greater than 20 m was revealed in the fault zone that extends along the eastern side of the Hula Basin; 15 m of this separation arose in the last 4–5 ka [40].

In most cases the roughly meridional direction of fracture systems is clearly expressed in local basins except for stations 0301, 0305, 0403, and 0405, where the general trend is suppressed by diagonal fault systems, two of which (0301 and 0403) exactly fall into NE- and NW-trending fault zones. On the contrary, in the interbasin links south and north of Lake Kinneret, no fracture maximums that would fit the rift direction were noticed at three (0601, 0603, and 0701) of the four stations.

Fracture systems with W–E, NE, and NW orientations are much less frequent (Fig. 5A, see the rose diagram); among these most are spread 310–320° and 340–350° NW, 270–280° W, and, to a lesser extent, 40–50° NE. Mesostructural attributes indicate normal (0403, 0401, 0405, and 0601) and strike-slip and normal (0301) displacements along the NW faults, strike-slip displacements (0302) along latitudinal faults, and strike-slip (0301, 0305) and normal displacements (0301 and 0703) along NE-trending faults (Fig. 4).

To estimate the significance of particular fracture systems, their strike azimuths were plotted versus intensity I of their maximums (Fig. 5A). The plot clearly demonstrates that the meridional and northwestern fracture systems reveal the highest intensity in comparison with all other directions. Maximum intensity I in the southern (the western coast of the Gulf of Elat and the Arava Valley) and central (Dead Sea Basin) parts of the study area is higher than in the northern part (the Lake Kinneret and Hula basins and adjacent offsets). Station 0702 is the only exception.

A similar statistical processing was conducted for fault zones whose spatial characteristics and widths of crush and fracture zones, W, were measured during field studies. As can be seen from the rose diagram shown in Fig. 5B, the meridional (0–10°) faults head the list and the NW fractures (330–340°) rank second. The NE

Fig. 4. Location of stations in the study area and related fracture diagrams (projection of the upper hemisphere). Window size is 10°. Contour lines of fracture density are drawn at 3.5, 7.5, 9.5, and greater percents. Station number, number of measurements n, rock type, and its geologic age taken from geological map [32] are given below each diagram. Pairs of conjugated fracture systems in diagrams are denoted by Roman numerals. (*1*) Station; (*2*) uplift axis; (*3*) border of Israel; (*4*) downdip striation with declination angles 60–90°; (*5*) oblique striation with declination angles 30–60°; (*6*) nearly horizontal striation with declination angles 0–30°; (*7*) downdip displacement of markers; and (*8*) lateral displacement of markers.

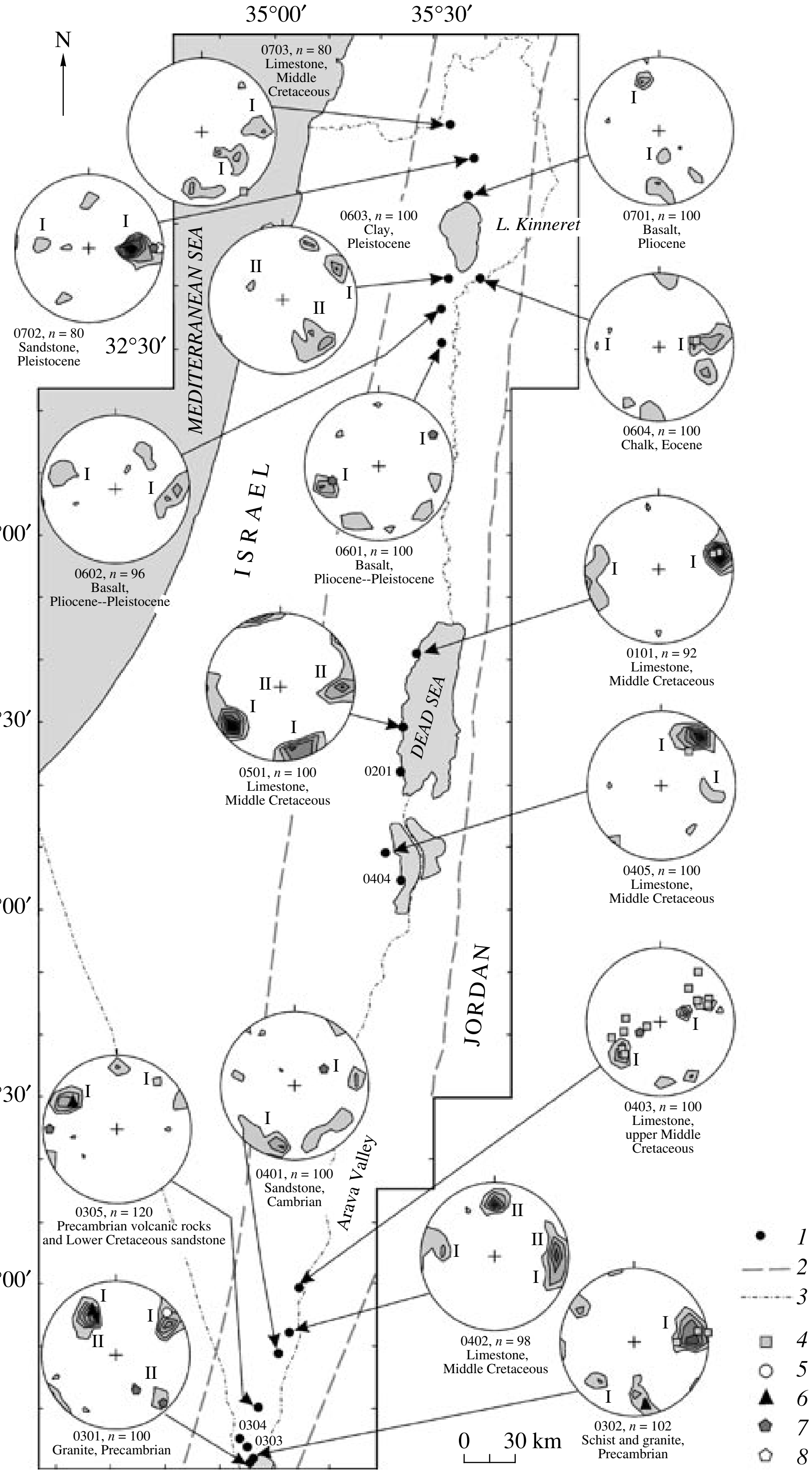
35°00′
35°30′
N
0703, n = 80
Limestone,
Middle
Cretaceous
0702, n = 80
Sandstone,
Pleistocene
32°30′
0603, n = 100
Clay,
Pleistocene
L. Kinneret
0701, n = 100
Basalt,
Pliocene
0604, n = 100
Chalk, Eocene
MEDITERRANEAN SEA
0602, n = 96
Basalt,
Pliocene--Pleistocene
I S R A E L
0601, n = 100
Basalt,
Pliocene--Pleistocene
32°00′
0101, n = 92
Limestone,
Middle Cretaceous
31°30′
0501, n = 100
Limestone,
Middle Cretaceous
DEAD SEA
0201
0405, n = 100
Limestone,
Middle Cretaceous
0404
31°00′
JORDAN
0403, n = 100
Limestone,
upper Middle
Cretaceous
30°30′
0305, n = 120
Precambrian volcanic rocks
and Lower Cretaceous sandstone
0401, n = 100
Sandstone,
Cambrian
Arava Valley
30°00′
0402, n = 98
Limestone,
Middle Cretaceous
0301, n = 100
Granite, Precambrian
0304
0303
0 30 km
0302, n = 102
Schist and granite,
Precambrian
1
2
3
4
5
6
7
8

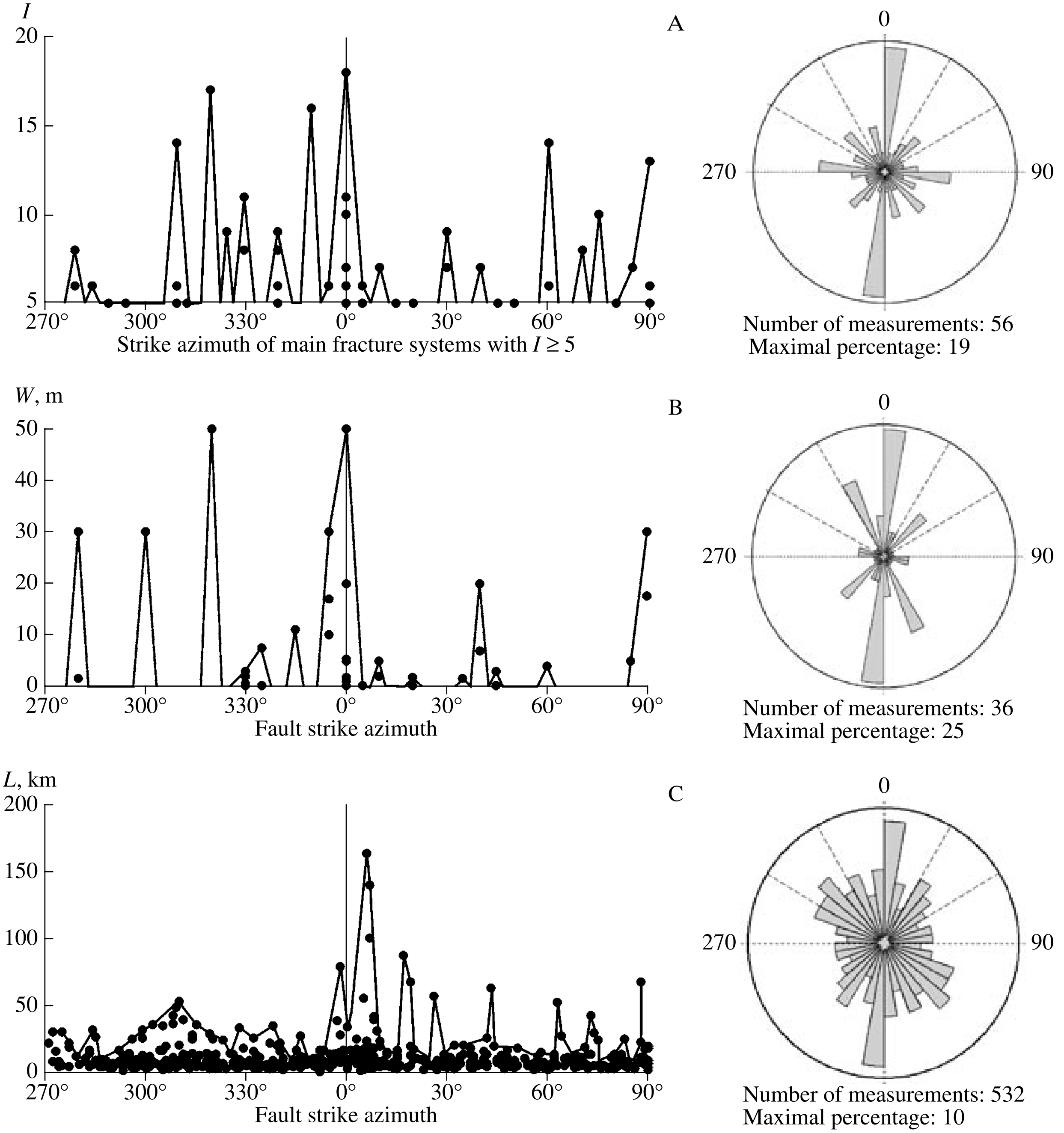

Fig. 5. Statistically processed structural data: (A) intensity I of main fracture systems with $I \geq 5$ (see Fig. 4) versus strike azimuth and the related rose diagram, (B) thickness of crush and fracture zones (W) measured at stations versus strike azimuth and the related rose diagram, and (C) fault length L measured at uplifts limited by their axes (see Fig. 3) versus strike azimuths and the related rose diagram.

faults (40–50°) are expressed more poorly, and the nearly latitudinal faults do not reveal significant maximums against the others. The distribution of strike azimuths versus the width of their fault zones also shows that the highest W values are typical of N–S and NW faults (Fig. 5B).

A similar analysis was carried out for strike azimuths and lengths L of faults (Fig. 5C). These parameters were taken from a structural map (Fig. 3). Moreover, only those faults that either are localized within the rift between uplift axes or transect them were involved in the processing. The master meridional direction (0–10°) again stands out in the rose diagram, and the longest faults are related to this direction. The NW-trending faults (290–340°) make up a rather diffuse maximum (Fig. 5C). The northeastern orientation

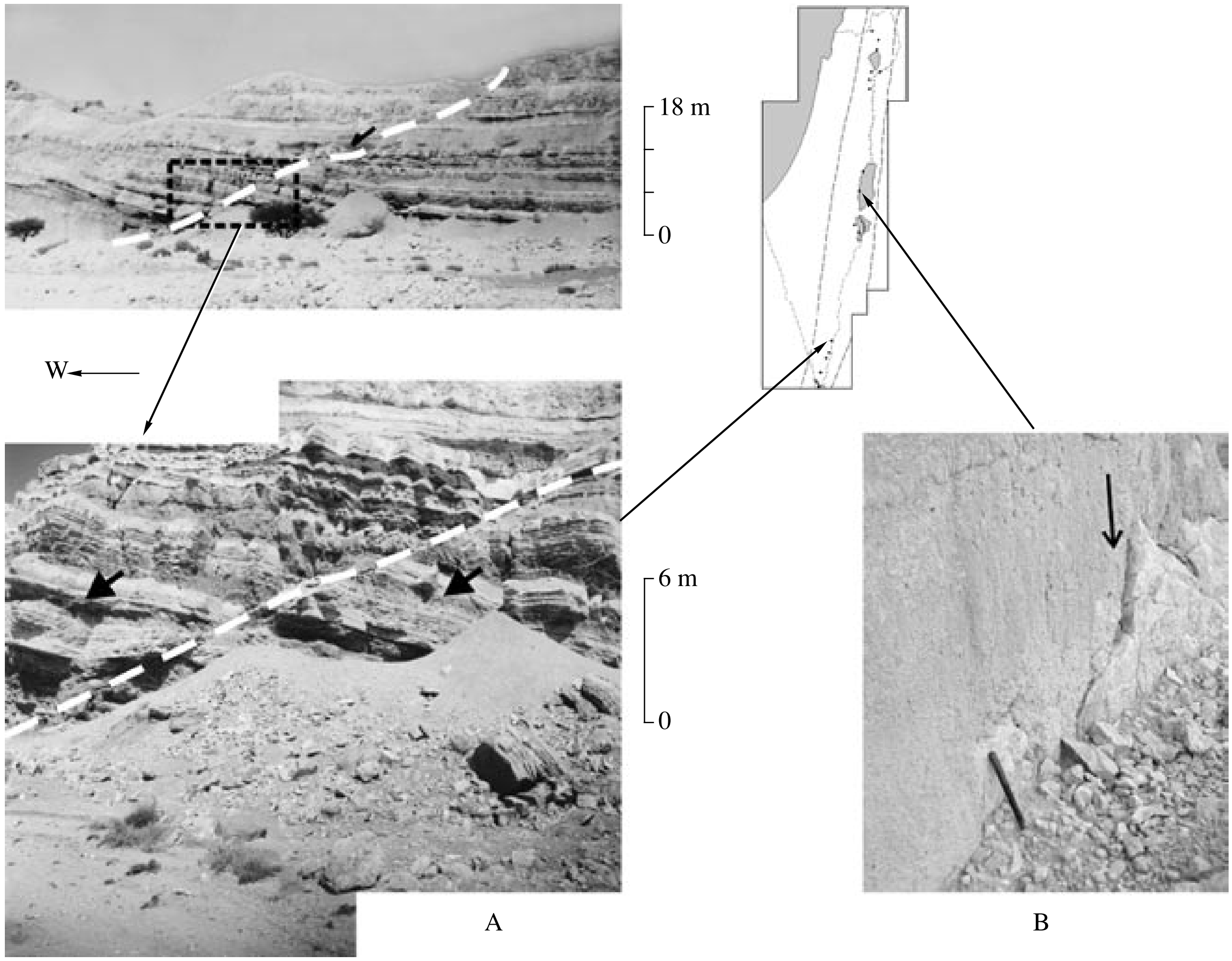

Fig. 6. Indications of vertical displacements along meridional faults: (A) normal displacements with an amplitude of 6 m along the fault zone with dip azimuth 240–270° SW ∠ 30–40° in intercalating limestone and clay in the western wall of the Arava Valley at Station 0403, and (B) downdip striation on a fracture plane with dip azimuth 75° NE ∠ 75–80° in limestone near the western coast of the Dead Sea at Station 0101.

of faults is somewhat suppressed, and the latitudinal faults are entirely lost against the faults oriented in other directions. The extents of variously trending auxiliary faults are approximately equal. In sporadic measurements, the length of W–E and NE faults exceeds the maximal recorded length of NW faults by 12–20 km, whereas in the general selection, the length of NW faults is commonly greater than that of their NE counterparts.

The statistical processing of fault and fracture parameters has shown that the structural grain in the southern Dead Sea Rift is largely controlled by the meridional master faults retaining a stable spatial orientation (0–10°) and by auxiliary, less abundant, NW-trending faults with azimuths varying from 290 to 340°. Systems of NE and W–E faults are of minor importance relative to the two systems mentioned above. The occurrence of a latitudinal maximum in the rose diagram for fractures and the absence of such a maximum in the rose diagram for faults indicate that the distribution of fractures does not always mirror the orientation of large faults and is often consistent with faults of lower hierarchical levels that do not form large fault zones. The meridional rifting probably arrested the development of latitudinal faults at some stages of regional tectonic evolution.

Stress Fields

Determination of conjugated fracture systems and direction of principal stress axes. The method proposed by J. Angelier [9] has been widely applied in recent years for reconstruction of stress fields. This method is based on the assumption that the slip along the fault plane occurs in the direction of maximum realized tangential stress. Striations on fracture planes are used for the stress field reconstruction. This method has several advantages; however, at least ten fractures with striation are required for obtaining a stress tensor that can characterize the state of stress in a rock massif. This

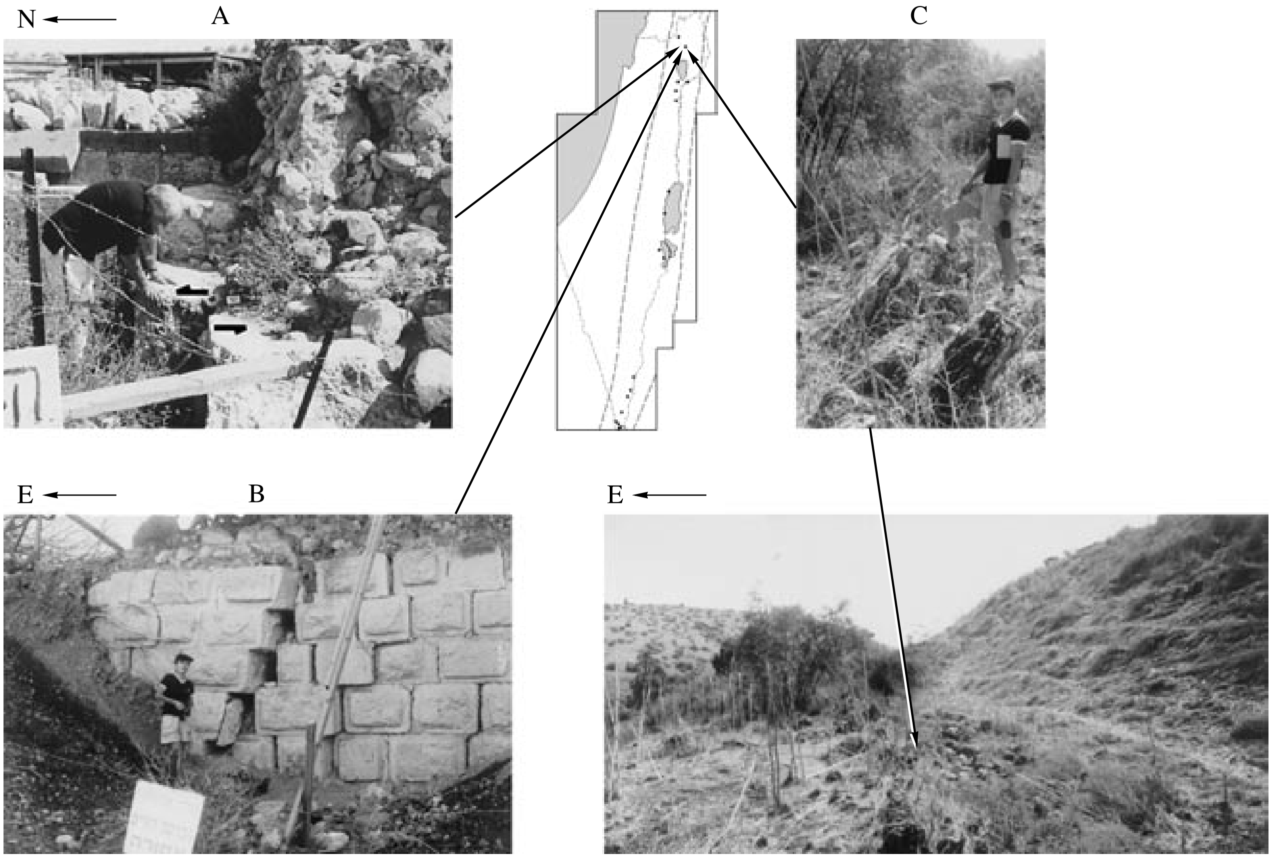

Fig. 7. Deformed walls of the Templar Castle of Vadum Iacob (built in 1187), situated between the Hula Basin and Lake Kinneret at Station 0702, and a nearby bedrock outcrop: (A) left-lateral displacement of 0.5 m; (B) severely deformed wall with indications of oblique displacements. Maximal gap of the fissure is 0.28 m, left-lateral slip is 0.23 m, normal separation is 0.07 m; (C) normal fault zone with apparent thickness of 1.0–1.5 m; dip azimuth 90° E ∠ 60° in Pleistocene sandstone, ~10 m downslope of the Templar Castle of Vadum Iacob.

requirement is not always fulfilled because striation is eliminated in some bedrocks with time owing to exogenic alteration and completely disappears in poorly cemented and loose sediments. In this case, the well-known relationships between the directions of principal normal stresses and the orientation of arising faults may be used for reconstruction of stress fields on the basis of fracture patterns even without a priori knowledge of the kinematics of displacements [1, 37]. These basic statements were used in this investigation.

In order to reliably estimate a state of stress with this classic method, one must establish conjugated shear systems that have been formed or reactivated simultaneously. The conjugated shear systems were selected during two stages. Initially, they were outlined from direct geological observations using traditional criteria of their conjugation, e.g., fracture merging, mutual cross-cutting relations, retention of a constant angle between fractures during a change of their orientation, similar regional abundance, and similar and coeval mineral fill [1, 37]. At the second stage, diagrams of fracture orientation were analyzed with the Nikolaev method [5] based on the systematic asymmetric scattering of maximums that arises in the common field of tectonic stresses (Figs. 8A, 8B). The main condition of fracture conjugation consists in the opposite direction of such scattering. Thereby, the maximums should be located approximately on the arc of a large circle, and the shearing angle between them must be no less than 30°. Thus, to restore the directions of principal stress axes, such fracture systems were used, the conjugation of which is confirmed by field and statistical criteria. Further reconstruction boiled down to simple geometric developments, which are well known from structural geology and tectonophysics (Figs. 8C, 8D).

Results of stress field reconstructions. It has been established that the state of stress in the southern Dead Sea Rift is characterized by three types of stress fields (Fig. 9). They are determined by relationships between inclinations of principal stress axes relative to the horizon [7]:

extension: $\sigma_1 = 60–90°$, $\sigma_2 = 0–30°$, and $\sigma_3 = 0–30°$;

shear: $\sigma_1 = 0–30°$, $\sigma_2 = 60–90°$, and $\sigma_3 = 0–30°$;

transtension: $\sigma_1 = 30–60°$, $\sigma_2 = 30–60°$, and $\sigma_3 = 0–30°$,

where σ_1 is the compression axis, σ_2 is the intermediate axis, and σ_3 is the extension axis.

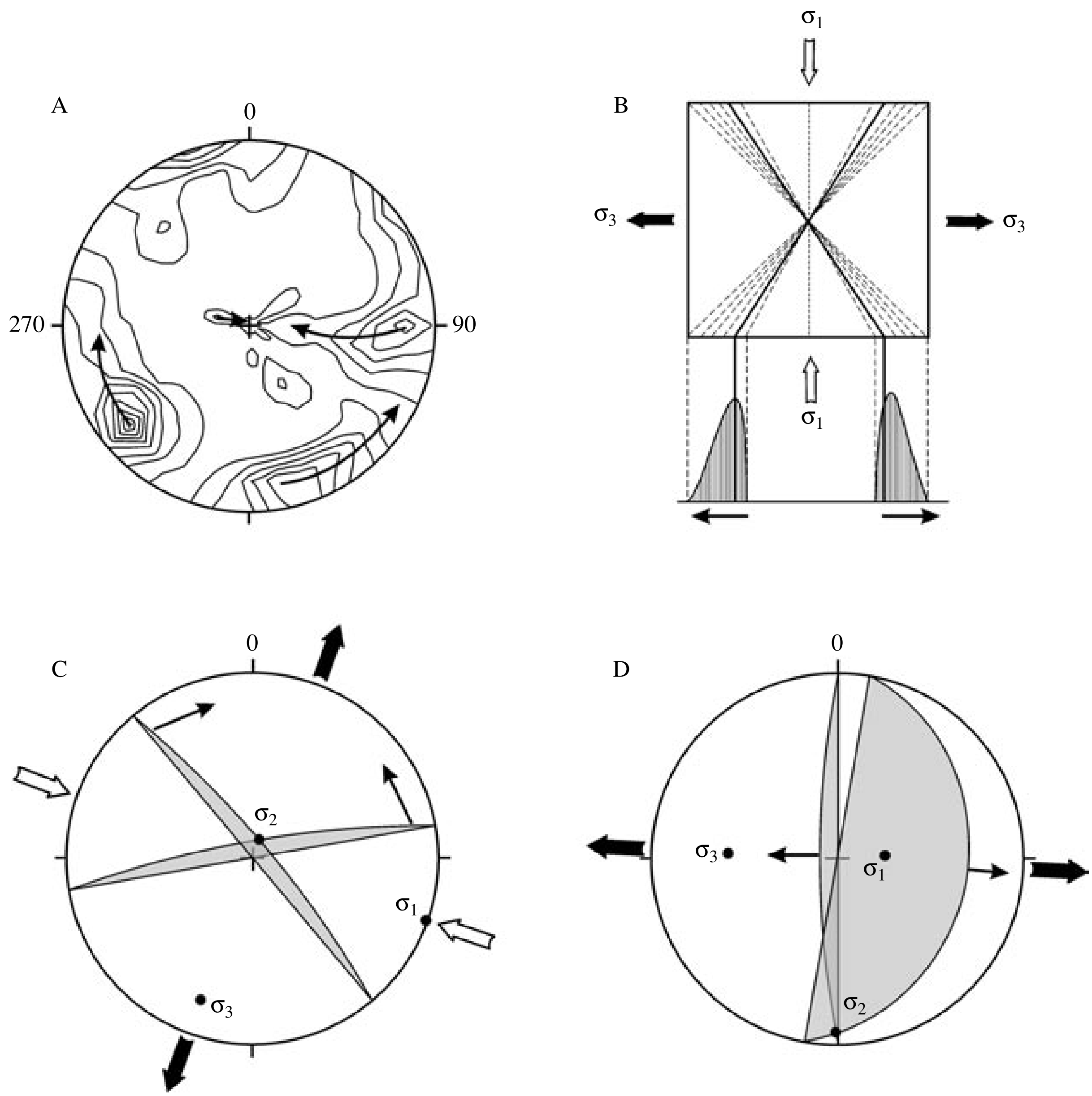

Fig. 8. Determination of conjugated fracture systems and reconstruction of principal normal stress axes. Station 0501, projection of the upper hemisphere. (A) Fracture diagram at Station 0501. Arrows indicate directions of prevalent scattering in maximums of fracturing that confirm conjugation of fracture systems [3]. Number of measurements is 100; window size is 10°. Contour lines are drawn at 0.5, 2.5, 4.5, 6.5%, and greater percentages. (B) Scheme of fracture scattering (shown by dashed lines) under compression (σ_1) and extension (σ_3), after [5]. (C and D) orientation of principal normal stresses: (σ_1) compression axis, (σ_2) intermediate axis, and (σ_3) extension axis.

Two solutions were obtained at 4 of the 16 stations. One of them corresponds to extension; the other, to shear deformation. The first and most abundant type that fits extension comprises 11 solutions, where the horizontal extension axis in most cases has a latitudinal orientation or slightly deviates from it in the counterclockwise direction. This stress field occurs in rocks of various ages and is best developed in the Pliocene–Pleistocene basalts and Pleistocene sediments exposed in the northern study territory. In the two solutions, the extension axis is oriented in the northwestern direction because of local variations of the state of stress or as a reflection of a short-term pre-Pleistocene stage.

The second group comprises eight shear solutions and one solution that fits transtension. The group is characterized by a scattered orientation of principal stresses. In three solutions related to the Precambrian, Cretaceous, and Pleistocene rocks, the extension axis is oriented in a nearly latitudinal direction (80–110°). In four solutions this axis is directed to the northeast (40–50° and

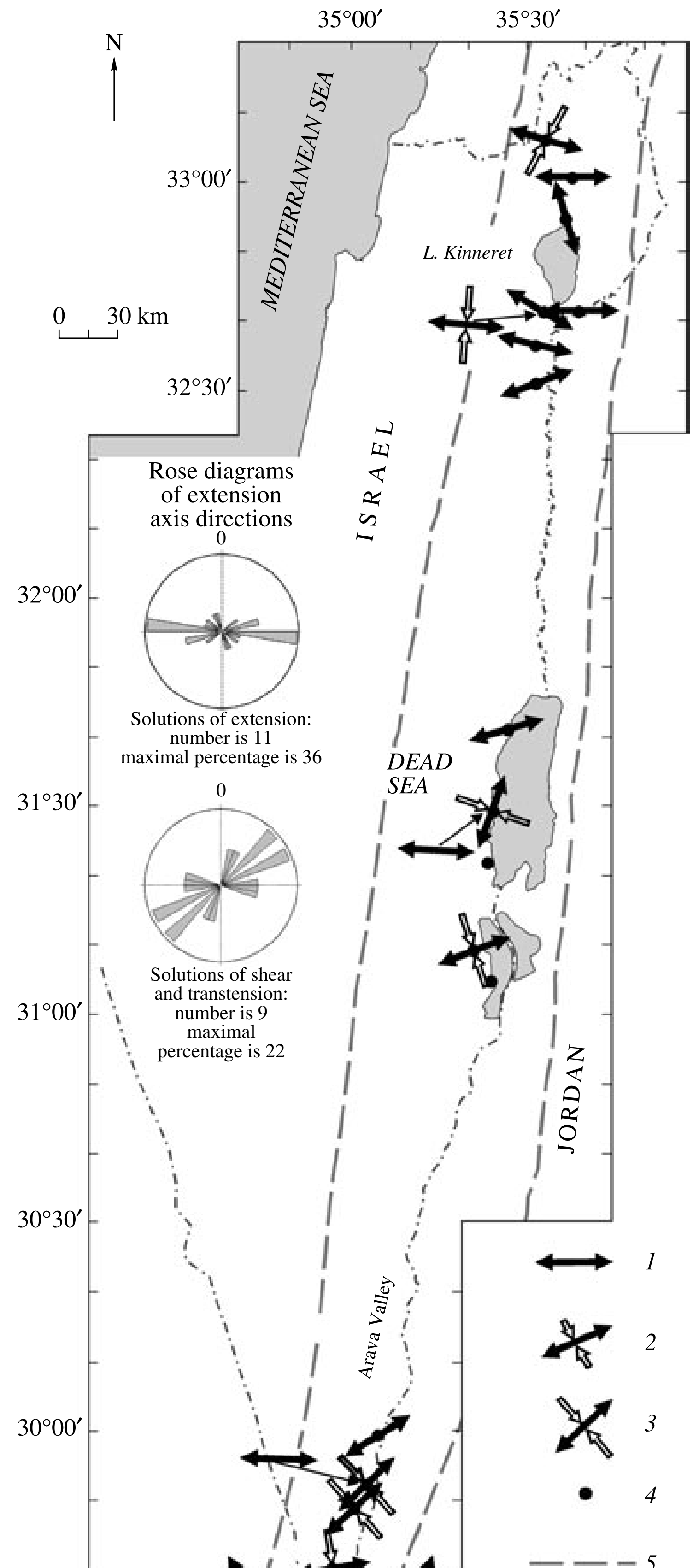

Fig. 9. Stress fields in the southern Dead Sea Rift as deduced from fracture distribution. Types of stress fields: (*1*) extension, (*2*) transtension, (*3*) shear; (*4*) station; (*5*) axes of uplifts on rift shoulders; and (*6*) border of Israel.

60–70°); in two solutions, to the north-northeast (10–30°). Accordingly, the axes of horizontal compression are perpendicular to the extension axes. The obtained results are close to those published by Eyal [17], who grouped the directions of principal horizontal stresses into two main paleotectonic regimes: (1) ENE extension and NNW compression associated with the Dead Sea Rift and (2) NNE extension and WNW compression related to the evolution of the Syrian Foldbelt since the Turonian. The data presented in this paper show that the first type of paleotectonic regime is predominant among shear fields within the rift in agreement with Eyal's statements. Moreover, exactly the NE orientation of axis σ_3 prevails in shear solutions. At the same time, the nearly latitudinal extension is also widely developed. Some authors assume that such an extension was the main driving force for the Dead Sea Rift formation [21, 31]. Both types of stress fields occur not only in Precambrian–Cretaceous but also in Pleistocene rocks. The focal mechanisms exhibiting strike-slip and normal faulting in earthquake sources [33, 38] suggest that they could also be typical of the modern stage.

It should be noted that fluctuations of the state of stress are more frequent in the southern study area than in the north, where the stress field demonstrates a relatively stable orientation of the principal axes. This difference probably reflects a specific structure of the Earth's crust in particular segments of the rift and its inhomogeneity in the segment that extends from the Gulf of Elat to the Dead Sea.

In general, the results of this investigation show that two main types of local stress fields are equally related to the structural evolution of the Dead Sea Rift: (1) W–E (predominant) and ENE extension and (2) a shear with NE (occasionally latitudinal) extension and NW (occasionally meridional) compression.

COMPARISON OF THE RESULTS OBTAINED WITH EXPERIMENTAL DATA AND DISCUSSION

Experimental studies provide insights into formation of natural structures. In particular, analog models have recently been successfully applied to the analysis of structural systems developing under conditions of shear, pure, and oblique extension [8, 10–13, 15, 16, 24, 26, 32, 36, 39]. Our data and their comparison with experimental results may shed light upon the developmental conditions and the geodynamic regime of the Dead Sea Rift.

The specific distribution of fault azimuths in oblique and orthogonal rifts and strike-slip zones is one of the obvious differences between them [8, 10, 12, 39]. As follows from experimental research, when rifting is orthogonal and angle α between the vector of extensional force and the rift axis is 90°, the fracture zones are represented by one system of normal faults oriented conformably to the strike of the forming structure [8, 12]. Scattering of fault azimuths steadily increases with a decrease in α, and the fault pattern substantially changes when $\alpha = 45°$ and 30°. The stable fault system arising in models deviates from the rift axis by 25–30° [8]. In the Dead Sea Rift, the NW maximum in the rose diagrams (Fig. 5) matches this system. The third fault system, oriented perpendicular to the rift axis and playing an important role in the rift infrastructure, appears at $\alpha = 30°$. This is expressed most clearly in the central block of the model [8], that is, in the axial portion of rift. As has been shown in this work, the latitudinal faults are not crucial for the internal structure of the Dead Sea Rift. The main, most extended faults of this orientation are concentrated in the southern part of the rift and should be regarded as special structures that were formed during the Eritrean Stage before intense downfaulting of the rift itself. This does not rule out their partial reactivation at the Levantine Stage when they could compensate extension [21]. Thus, comparison of experimental data with a real structural setting indicates that the oblique extension gave rise to the formation of two main fault systems of the meridional and the northwestern orientations that control the structure of the southern Dead Sea Rift.

Clifton *et al.* [12] showed that at $\alpha \geq 45°$ azimuths of the longest dislocations in models coincide with maximums of fault occurrence frequencies. To a certain extent, our data are consistent with this statement, because the most abundant fracture systems, the greatest widths of fault zones, and, in most cases, their lengths fit the maximums of fault azimuths in the rose diagrams (Fig. 5). At $\alpha = 30°$ and 45° these relationships are distorted. Hence, the vector of regional extension in the Dead Sea Rift is directed at an angle of 60–30° to its axis. As a result, the two prevalent types of stress field develop at a local level: (1) roughly latitudinal extension and (2) a shear with NE–SW orientation of the extension axis and NW–SE orientation of the compression axis (Fig. 9).

Thus, on the basis of the statistical processing of fault orientation, the fault systems that exist in the Dead Sea Rift may be regarded as similar to those obtained in models from oblique extension. The internal structure with en echelon arranged rift segments, valleys divided by interbasin links, is another specific feature of oblique rifts [26]. Such a structure is, in turn, emphasized by en echelon arranged faults with displacements varying from purely normal to strike-slip faulting [13]. In models, deformation is shared between different structures, and faults are generally steeper than in purely normal faults [36]. All these specific features are typical of the Dead Sea Rift and recognized in the structure of fault systems and topography.

The nearly meridional steeply dipping (70–80°) faults commonly typical of strike-slip dislocations and at the same time bearing evidence for normal faulting may serve as indications that the marked strike-slip displacements predated the intense rifting at the Levantine Stage. The meridional faults might have first developed as strike-slip structures. The subsequent prevalence of extension in the Earth's crust led to opening of the Dead Sea Rift, and this process also included the formation of normal faults with steep dip angles. Similar transitions of the state of stress from the strike-slip regime to extension have been established for the Baikal, Barguzin, and Kichera basins of the Baikal Rift Zone [30]. Taking this into account, one may agree with Sneh [34] that the lateral displacements in the late Oligocene and early Miocene preceded further downfaulting of the Dead Sea Rift. Nevertheless, this event could hardly lead to a horizontal slip for more than 100 km, as suggested by some authors [18, 19], because such a great lateral displacement would have remained as an indelible trace until now. As stated in this and other works, the Dead Sea Rift corresponds neither to the typical strike-slip fault nor to the pure rift but is most likely a result of oblique extension.

CONCLUSIONS

The performed structural studies have yielded new information concerning the fault systems and stress fields of the Dead Sea Rift within a segment from the Gulf of Elat to the Hula Basin. The comprehensive analysis with involvement of tectonophysical treatments has provided evidence for some features characterizing the setting of oblique extension:

(1) The fault network in the southern portion of the rift is largely controlled by meridional master faults steadily oriented 0–10° N and by auxiliary NW-trending faults (290–340° NW). Fault systems of other directions are less abundant and significant.

(2) Faults oriented in meridional and northwestern directions are the most extended and are accompanied by thick crush zones; the related fracture systems are characterized by the highest intensity.

(3) The meridional fracture systems are commonly best expressed within local basins, whereas in the interbasin links they are often suppressed by other fault systems.

(4) Mesostructural signs indicate normal faulting along nearly meridional faults within local basins while in the interbasin links the style of tectonic movements may change from normal to strike-slip faulting along the same rupture. The NW-trending faults are characterized by normal and normal–strike-slip displacements, the latitudinal faults reveal lateral separation, and the NE-trending faults demonstrate both strike-slip and normal displacements.

(5) Two main types of local stress fields are related to the tectonic evolution of the Dead Sea Rift: (1) extension of latitudinal (predominant) and ENE orientations and (2) a shear with NE (occasionally latitudinal) extension and NW (occasionally meridional) compression.

ACKNOWLEDGMENTS

I thank S.I. Sherman and Y. Mart for their assistance in this study, A.S. Gladkov for his helpful comments on the manuscript, and V.S. Burtman and M.L. Kopp for the valuable criticism and recommendations in their reviews. This work was supported by the University of Haifa, Israel, and by the Russian Foundation for Basic Research, project no. 04-05-64348.

REFERENCES

1. M. V. Gzovskii, *Principles of Tectonophysics* (Nedra, Moscow, 1975) [in Russian].
2. V. S. Imaev, L. P. Imaeva, and B. M. Koz'min, *Active Faults and Seismotectonics of Northeastern Yakutia* (Yakut. Sci. Center, Acad. Sci. USSR, Yakutsk, 1990) [in Russian].
3. M. L. Kopp, Zh. Adzhamyan, K. Il'yas, *et al.*, "Formation Mechanism of the El Ghab Wrench Graben (Syria) and the Levant Transform Fault Propagation," Geotektonika **33** (5), 77–92 (1999) [Geotectonics **33** (5), 408–422 (1999)].
4. M. L. Kopp, Yu. G. Leonov, and Zh. Adzhamyan, "Deformations of the West Arabian Platform as a Result of Strike-Slip Movements along the Levant Fault," Geotektonika **29** (3), 61–76 (1994).
5. P. N. Nikolaev, *Techniques of Tectonodynamic Analysis*, Ed. by N. I. Nikolaev (Nedra, Moscow, 1992) [in Russian].
6. S. N. Chernyshev, *Fractures in Rocks* (Nauka, Moscow, 1983) [in Russian].
7. S. I. Sherman and Yu. I. Dneprovskii, *Crustal Stress Fields and Geostructural Methods of Their Studies* (Nauka, Novosibirsk, 1989) [in Russian].
8. S. I. Sherman, K. Zh. Seminskii, S. A. Bornyakov, A. N. Adamovich, P. M. Lobatskaya, S. B. Lysak, and K. G. Levi, *Faulting in the Lithosphere. Extension Zones* (Nauka, Novosibirsk, 1992) [in Russian].
9. J. Angelier, "Fault Slip Analysis and Paleostress Reconstruction," in *Continental Deformation* (Pergamon, Oxford, 1994), pp. 101–120.
10. M. Bonini, Th. Souriot, M. Boccaletti, and J. P. Brun, "Successive Orthogonal and Oblique Extension Episodes in a Rift Zone: Laboratory Experiments with Application to the Ethiopian Rift," Tectonics **16** (2), 347–362 (1997).
11. J. P. Brun and V. Tron, "Development of the North Viking Graben: Inferences from Laboratory Modeling," Sediment. Geol. **86**, 31–51 (1993).
12. A. E. Clifton, R. W. Schlische, M. O. Withjack, and R. V. Ackermann, "Influence of Rift Obliquity on Fault-Population Systematics: Results of Experimental Clay Models," J. Struct. Geol. **22** (10), 1491–1509 (2000).
13. G. Corti, M. Bonini, F. Innocenti, *et al.*, "Centrifuge Models Simulating Magma Emplacement during Oblique Rifting," J. Geodynamics **31** (5), 557–576 (2001).
14. A. N. Darkal, M. Krauss, and R. Ruske, "The Levant Fault Zone. An Outline of Its Structure, Evolution, and Regional Relationship", Z. Geol. Wiss. **18** (6), 549–562 (1990).

15. O. Dauteuil and J. P. Brun, "Oblique Rifting in a Low Spreading Ridge," Nature **361**, 145–148 (1993).
16. O. Dauteuil and J. P. Brun, "Deformation Partitioning in a Slow Spreading Ridge Undergoing Oblique Extension: Mohns Ridge, Norwegian Sea," Tectonics **15** (5), 870–884 (1996).
17. Y. Eyal, "Stress Field Fluctuations along the Dead Sea Rift since the Middle Miocene," Tectonics **15** (1), 157–170 (1996).
18. R. Freund, Z. Garfunkel, I. Zak, *et al.*, "The Shear along the Dead Sea Rift," R. Soc. London Phil. Trans., No. A267, 107–130 (1970).
19. Z. Garfunkel, "Internal Structure of the Dead Sea Leaky Transform (Rift) in Relation to Plate Kinematics," Tectonophysics **80** (1), 81–108 (1981).
20. A. Heimann, M. Eyal, and Y. Eyal, "The Evolution of Barahta Rhomb-Shaped Graben, Mount Hermon, Dead Sea Transform," Tectonophysics **180** (1), 101–110 (1990).
21. A. Horowitz, A. Flexer, A. Ginzburg, Z. Ben-Avraham, and Z. Garfunkel, *The Jordan Rift Valley* (Balkema, Lisse, 2001).
22. E. L. Kashai and P. F. Croker, "Structural Geometry and Evolution of the Dead Sea-Jordan Rift System as Deduced from New Subsurface Data," Tectonophysics **141** (1), 33–60 (1987).
23. J. Letouzey and P. Tremolieres, "Paleo-Stress Fields around Mediterranean Derived from Microtectonics: Comparison with Plate Tectonic Data," Rock Mechanics **9**, 173–192 (1980).
24. K. R. McClay and M. J. White, "Analogue Modeling of Orthogonal and Oblique Rifting," Marine Petrol. Geol. **12** (2), 137–151 (1995).
25. Y. Mart, "The Dead Sea Rift, a Leaky Transform Fault or an Oblique Spreading Centre: a Short Review," Africa Geosci. Review **1** (4), 567–578 (1994).
26. Y. Mart and O. Dauteuil, "Analogue Experiments of Propagation of Oblique Rifts," Tectonophysics **316** (1–2), 121–132 (2000).
27. Y. Mart and A. Horowitz, "The Tectonics of the Timna Region in Southern Israel and the Evolution of the Dead Sea Rift," Tectonophysics **79**, 165–199 (1981).
28. Y. Mart and P. D. Rabinowitz, "The Northern Red Sea and the Dead Sea Rift," Tectonophysics **124** (1), 85–113 (1986).
29. L. Y. Picard, U. Golani, Y. K. Bentor, *et al.*, *Israel Geological Map. Scale 1 : 250000* (Geol. Surv. Israel, 1965, reprinted in 1999).
30. V. San'kov, A. Miroshnichenko, K. Levi, *et al.*, "Cenozoic Stress Field Evolution in the Baikal Rift Zone," Bull. Centre Rech. Elf Explor. Prod. **21** (2), 435–455 (1997).
31. A. Sagy and Z. Reches, "Fault Pattern, Joint Systems and Slip Partitioning along the Western Margins of the Dead Sea Rift," in *Proceedings of the First Stephan Mueller Conference on Dead Sea* (Eur. Geophys. Soc., 2000), p. 34.
32. S. D. Scott and V. Benes, "Oblique Rifting in the Havre Trough and Its Propagation into the Continental Margin of New Zealand: Comparison with Analogue Experiments," Marine Geophys. Res. **18**, 189–201 (1996).
33. A. Shapira, "Seismicity of the Dead Sea Basin," in *The Dead Sea, the Lake and Its Setting* (Oxford Univ. Press, Oxford, 1997), pp. 82–86.
34. A. Sneh, "The Dead Sea Rift: Lateral Displacement and Downfaulting Phases," Tectonophysics **263** (1–4), 277–292 (1996).
35. A. Sneh, Y. Bartov, T. Weissbrod, and M. Rosensaft, *Geological Map of Israel. Scale 1 : 200000* (Geol. Surv. Israel, 1998).
36. V. Tron and J. P. Brun, "Experiments on Oblique Rifting in Brittle–Ductile Systems," Tectonophysics **188**, 71–84 (1991).
37. R. J. Twiss and E. M. Moores, *Structural Geology* (Freeman and Co., New York, 1992).
38. T. Van Eck and R. Hofstetter, "Fault Geometry and Spatial Clustering of Microearthquakes along the Dead Sea–Jordan Rift Fault Zone," Tectonophysics **180** (1), 15–27 (1990).
39. M. O. Withjack and W. R. Jamison, "Deformation Produced by Oblique Rifting," Tectonophysics **126**, 99–124 (1986).
40. E. Zilberman, R. Amit, A. Heimann, and N. Porat, "Changes in Holocene Paleoseismic Activity in the Hula Pull-Apart Basin, Dead Sea Rift, Northern Israel," Tectonophysics **321** (2), 237–252 (2000).

Reviewers: M.L. Kopp and V.S. Burtman